https://doi.org/10.30799/jnst.S309.26110409 J. Nanosci. Tech. - Volume 11 Issue 4 (2026) 1153–1156

Share Your Innovations through JACS Directory

Journal of Nanoscience and Technology

Visit Journal at https://www.jacsdirectory.com/jnst

ISSN: 2455-0191

Synthesis and Characterizations of CeO_2-TiO_2 Nanocomposites for Gas Sensing Applications

Hrutuja A. Patil, Gokul V. Suryawanshi*, Tulshidas S. Savale

Dept. of Chemistry, M.G.V's M.S.G. Arts, Science and Commerce College, Malegaon Camp, Malegaon, Nashik – 423 105, Maharashtra, India.

ARTICLEDETAILS

Article history:
Received 24 February 2026
Accepted 11 March 2026
Available online 15 April 2026

Keywords:
TiO_2–CeO_2
Nanocomposites
Sol Gel
Gas Sensor
Nanocrystal

ABSTRACT

TiO_2–CeO_2 nanocomposites were successfully synthesized using the sol–gel method, which is a flexible, cost-effective, and widely adopted chemical synthesis technique known for producing highly homogeneous and ultra-pure nanostructured materials. The sol–gel process allows precise control over composition, particle size, and microstructure, making it particularly suitable for preparing mixed metal oxide nanocomposites. In recent years, the TiO_2–CeO_2 system has attracted considerable research interest due to its synergistic physicochemical properties, which enhance its performance in applications such as photocatalysis, environmental remediation, gas sensing, and energy-related technologies. In the present study, titanium isopropoxide and cerium nitrate were used as precursor materials for titanium and cerium sources, respectively. These precursors were hydrolyzed under carefully controlled pH and temperature conditions to obtain TiO_2–CeO_2 nanocomposites with varying molar ratios of TiO_2 and CeO_2. Controlled hydrolysis and condensation reactions ensured uniform distribution of CeO_2 within the TiO_2 matrix. The resulting sols gradually transformed into gels, which were subsequently aged to improve network formation and structural stability. X-ray diffraction (XRD) analysis confirmed the successful formation of anatase TiO_2 and fluorite-structured CeO_2 phases. The absence of impurity peaks in the diffraction patterns indicated high phase purity and effective incorporation of CeO_2 into the TiO_2 lattice. The crystallite size of the nanocomposites was found to vary between 10 and 25 nm, depending on the CeO_2 content and the calcination temperature, suggesting that cerium doping influenced crystal growth and inhibited particle agglomeration. Fourier-transform infrared spectroscopy (FTIR) was employed to analyze the chemical bonding and functional groups present in the nanocomposites. The FTIR spectra exhibited characteristic metal–oxygen stretching vibrations corresponding to Ti–O–Ti, Ce–O, and Ti–O–Ce bonds. These features confirmed strong chemical interactions and successful coupling between TiO_2 and CeO_2 within the nanocomposite structure. Field emission scanning electron microscopy (FE-SEM) revealed nearly spherical nanoparticles with relatively uniform size distribution and reduced agglomeration. UV–visible diffuse reflectance spectroscopy (UV–Vis DRS) indicated enhanced optical absorption and band-gap modification due to CeO_2 incorporation.

1. Introduction

Titanium dioxide (TiO_2) is one of the most widely investigated photocatalysts for the degradation of organic pollutants due to its high photochemical stability, strong oxidizing capability, non-toxicity, low cost, and abundant availability [1]. TiO_2 exists mainly in three crystalline polymorphs: anatase, rutile, and brookite. Among these, anatase typically exhibits superior photocatalytic performance, attributed to its larger specific surface area and reduced rate of photoinduced charge carrier recombination [2,3]. However, the practical efficiency of pristine TiO_2 remains limited by its wide band gap (~3.2 eV), which restricts light absorption predominantly to the ultraviolet region of the solar spectrum, representing only a small fraction of incident solar energy [4,5]. Moreover, the rapid recombination of photogenerated electron–hole pairs significantly diminish quantum efficiency [6]. To address these limitations, various modification strategies have been explored, including morphological control, surface sensitization, ion doping, and coupling with other semiconductors [7]. Among these approaches, forming heterostructures with cerium dioxide (CeO_2) has emerged as a promising route for enhancing photocatalytic activity [8]. CeO_2, a lanthanide oxide with reversible Ce^{3+}/Ce^{4+} redox behaviour and high oxygen storage capacity, can facilitate charge separation and promote interfacial charge transfer when integrated with TiO_2 [9]. The creation of TiO_2–CeO_2 heterojunctions not only suppresses electron–hole recombination but also extends optical absorption toward the visible region [10,11]. Additionally, oxygen vacancies and defect sites introduced by CeO_2 contribute to improved adsorption and surface reactivity [12]. In this context, the sol–gel method offers a versatile synthesis route, enabling precise control over composition, homogeneity, and particle size at relatively low temperatures [13]. The present study focuses on the sol–gel synthesis, characterization, and photocatalytic evaluation of CeO_2/TiO_2 nanocomposites to elucidate the influence of cerium incorporation on structural, optical, and photocatalytic properties [14]. It also has a high oxygen storage capacity. By creating heterojunctions at the TiO_2–CeO_2 interface, the addition of CeO_2 to TiO_2 not only increases light absorption into the visible spectrum but also efficiently reduces electron–hole pair recombination [15]. This cooperative relationship improves the composite material's photocatalytic effectiveness and helps keep it stable over several catalytic cycles [16]. Additionally, CeO_2 can introduce defect sites and oxygen vacancies that act as active foci for adsorption and interaction with pollutant molecules, increasing the total photocatalytic activity [17]. Due to its ability to precisely control composition, homogeneity, and particle size at relatively low temperatures, the sol-gel method of synthesizing TiO_2–CeO_2 nanocomposites has garnered increased attention in recent years [18,19].

2. Experimental Methods

2.1 Synthesis of TiO_2-NPs

Nitric acid (HNO_3) and titanium tetra isopropoxide (TTIP, Sigma-Aldrich, 97%) were used as received without further purification. $Ce(NO_3)_3{\cdot}6H_2O$ and titanium butoxide [$Ti(OBu)_4$] served as cerium and titanium precursors, respectively. Initially, 10 mL of $Ti(OBu)_4$ was dissolved in 10 mL of anhydrous alcohol and ultrasonically dispersed. The

*Corresponding Author:gklsuryawanshi24@gmail.com(Gokul V. Suryawanshi)

https://doi.org/10.30799/jnst.S309.26110409

Cite this Article as: Hrutuja A. Patil, Gokul V. Suryawanshi, Tulshidas S. Savale, Synthesis and characterizations of CeO_2-TiO_2 nanocomposites for gas sensing applications, J. Nanosci. Tech. 11(4) (2026) 1153–1156.

Ti precursor solution was then added dropwise to the $Ce(NO_3)_3{\cdot}6H_2O$ solution at the desired Ce/Ti molar ratio (1/0.05/0.10). The mixture was stirred for 2 h at room temperature, and the pH was adjusted to 10 using ammonia solution, resulting in the formation of a yellow sol. The sol was aged for 24 h, followed by filtration, washing with deionized water and anhydrous alcohol, and drying at 100 °C for 12 h. The dried precursor was calcined at 600 °C for 4 h in air to obtain nanocrystallineCeO_2/TiO_2 composite powder.

2.2 Synthesis of CeO_2 NPS

Cerium oxide (CeO_2) nanoparticles were synthesized via the sol–gel technique using cerium nitrate hexahydrate, Cerium nitrate hexahydrate [$Ce(NO_3)_3{\cdot}6H_2O$], as the precursor. Initially, 4.34 g of $Ce(NO_3)_3{\cdot}6H_2O$ (molar mass ≈ 434.22 $gmol^{-1}$) was accurately weighed and dissolved in 100 mL of deionized water under continuous magnetic stirring at room temperature to obtain a 0.1 M solution. A suitable chelating/stabilizing agent such as citric acid (molar ratio 1:1 with cerium nitrate; ~1.92 g) or ethylene glycol (few mL, depending on desired viscosity) was added to promote homogeneous mixing and regulate hydrolysis. The solution was stirred until a clear and uniform sol was formed. The sol was then aged at room temperature for 12–24 h to allow gel formation via polycondensation reactions. The resulting gel was dried at 80–100 °C for 10–12 h to remove residual solvent and moisture. Finally, the dried gel was calcined at 600 °C for 3 h in air to obtain crystalline CeO_2 nanoparticles. The calcination step enabled decomposition of organic constituents and crystallization of CeO_2. The synthesized nanoparticles typically exhibit high crystallinity, nanoscale particle size, and abundant oxygen vacancies, which are advantageous for catalytic and gas-sensing applications.

2.3 Synthesis of CeO_2-TiO_2 Nanocomposites

CeO_2/TiO_2 composite nanoparticles were synthesized via a controlled sol–gel method using titanium(IV) butoxide ($Ti(OBu)_4$) and cerium nitrate hexahydrate ($Ce(NO_3)_3{\cdot}6H_2O$) as titanium and cerium precursors, respectively. Initially, $Ti(OBu)_4$ was dissolved in anhydrous alcohol under continuous stirring and ultrasonication to ensure complete homogenization. Separately, an aqueous solution of $Ce(NO_3)_3{\cdot}6H_2O$ was prepared and added dropwise to the Ti precursor solution while maintaining the desired Ce/Ti molar ratio. The slow addition facilitated uniform mixing and controlled hydrolysis during sol formation. The pH of the reaction mixture was adjusted to ~10 using ammonia solution to promote gelation. The resulting gel was filtered and thoroughly washed with deionized water and anhydrous alcohol to remove residual impurities and unreacted species. Finally, the purified gel was dried at 100 °C for 12 h to obtain CeO_2/TiO_2 composite nanoparticles.

3. Results and Discussion

3.1 UV–Visible Analysis

The UV–Visible absorption behaviour of CeO_2–TiO_2 nanoparticles is presented in Fig. 1. The UV–Vis absorption spectrum of the CeO_2–TiO_2 nanocomposite exhibits a strong and broad absorption band in the deep-UV region, beginning around 200 nm with an absorbance of approximately 1.45–1.50, which reflects the intrinsic electronic transitions of both TiO_2 and CeO_2. The high absorption intensity arises mainly from $O^{2-} \rightarrow Ti^{4+}$ and $O^{2-} \rightarrow Ce^{4+}$ charge-transfer transitions, and it signifies the formation of nanoscale semiconductor domains with a wide band gap. As the wavelength increases, a gradual decrease in absorbance occurs, followed by a prominent drop near 350–380 nm, corresponding to the fundamental absorption edge of the composite. This region represents the combined band-gap behavior of TiO_2 (≈3.2 eV) and CeO_2 (≈3.1–3.2 eV).

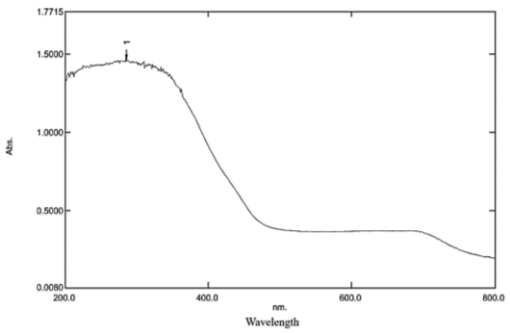

Fig. 1 UV–visible absorption spectrum of synthesized CeO_2–TiO_2 nanoparticles

The slight tailing of the absorption edge into the visible region indicates the presence of Ce-induced defect states, oxygen vacancies, and electronic coupling at the CeO_2–TiO_2 interface. Such effects often result in marginal band-gap narrowing, improved light harvesting, and enhanced charge separation. Beyond 450 nm, the spectrum flattens at a lower absorbance level, with a weak hump observed near 700–750 nm, which can be attributed to defect-related transitions or localized Ce^{3+} states. Overall, the UV–Vis profile confirms successful formation of the CeO_2–TiO_2 nanocomposite, improved interaction between the two oxide phases, and the presence of structural defects that can significantly enhance photocatalytic activity, UV-driven processes, and gas-sensing performance due to better electron–hole separation and increased surface reactivity.

3.2 FE-SEM Analysis

The surface morphology and particle size distribution of the synthesized CeO_2–TiO_2 nanoparticles are shown in Fig. 2. The FE-SEM micrographs of the CeO_2–TiO_2 nanocomposite exhibit a highly agglomerated surface morphology composed of densely packed nanosized particles. At lower magnification, the sample shows irregular clusters and grain-like structures, indicating strong inter-particle interaction driven by high surface energy and the inherent tendency of CeO_2 and TiO_2 nanoparticles to agglomerate. The TiO_2 component appears as flower-like or plate-like crystalline aggregates in some regions, while CeO_2 nanoparticles form smaller granular structures surrounding and interconnecting these clusters. This mixed morphology confirms successful composite formation, where TiO_2 crystallites act as a structural backbone while CeO_2 nanoparticles deposit on or between TiO_2 surfaces, increase surf roughness and active sites.

Higher-magnification images further reveal that the nanocomposite consists of uniformly distributed spherical to near-spherical nanoparticles with an average particle size in the range of ~20–33 nm, as indicated by the measurements shown in the images (values such as 21.6, 22.9, 24.3, 25.6, 27.0, 28.4, 33.0 nm). The particle size variation suggests the coexistence of both CeO_2 and TiO_2 nanoscale domains, where TiO_2 typically forms slightly larger crystalline grains and CeO_2 contributes smaller particles. The rough and porous texture observed throughout the microstructure indicates high surface area, which is beneficial for catalytic and gas-sensing applications, because it allows easier gas diffusion and more active adsorption sites.

Overall, the FE-SEM analysis confirms the successful synthesis of the CeO_2–TiO_2 nanocomposite with nanoscale particle distribution, heterogeneous morphology, and strong agglomeration. The combination of granular CeO_2 nanoparticles with plate- or flower-like TiO_2 structures significantly enhances the surface complexity, which is expected to improve gas sensitivity and catalytic reactivity due to better charge transfer across CeO_2–TiO_2 heterojunctions and increased surface-active regions.

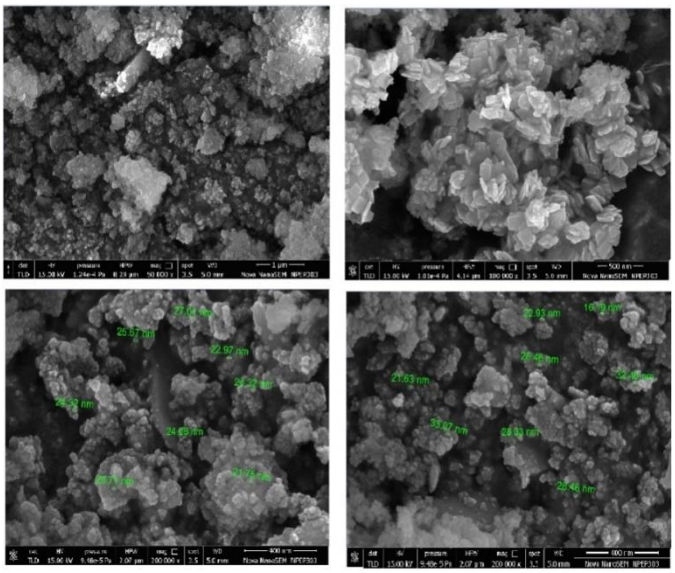

Fig. 2 SEM micrographs of synthesized CeO_2–TiO_2 nanoparticles

3.3 EDS Analysis

The EDS spectrum clearly displays characteristic peaks corresponding to cerium (Ce), titanium (Ti), and oxygen (O), confirming the successful formation of the CeO_2–TiO_2 nanocomposite without any notable impurity elements. A strong Ti peak appears around 4.5 keV, along with a secondary

https://doi.org/10.30799/jnst.S309.26110409

Cite this Article as: Hrutuja A. Patil, Gokul V. Suryawanshi, Tulshidas S. Savale, Synthesis and characterizations of CeO_2-TiO_2 nanocomposites for gas sensing applications, J. Nanosci. Tech. 11(4) (2026) 1153–1156.

Ti signal near 3.2 keV, both corresponding to Ti K-series emissions typical of TiO_2. Cerium shows multiple well-defined peaks in the 0.9–1.2 keV and 4.8–5.5 keV regions, indicating the presence of Ce Lα and Ce Lβ transitions, which are expected for CeO_2. Oxygen contributes a prominent low-energy peak near 0.5 keV, confirming oxide formation and matching the expected stoichiometry for mixed metal oxides.

The proportional intensities of Ce, Ti, and O peaks suggest that both metal oxides are well-distributed within the sampled region, supporting the FE-SEM observations that showed an integrated and uniform composite structure. The absence of unwanted elements such as carbon, sodium, chlorine, or transition-metal contaminants indicates that the synthesis process was clean and free from residual precursors. The elemental composition was confirmed by EDX analysis (Fig. 3).

Overall, the EDS analysis provides strong evidence for the successful incorporation and coexistence of CeO_2 and TiO_2 within the nanocomposite, reinforcing its suitability for applications like gas sensing, catalysis, and UV-driven processes where purity and elemental homogeneity significantly influence performance.

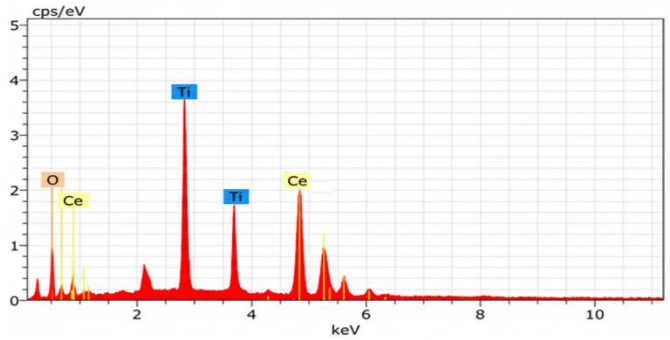

Fig. 3 Energy dispersive X-ray (EDX) spectrum of synthesized TiO_2–CeO_2 nanocomposite showing characteristic peaks of Ti, Ce, and O elements, confirming the elemental composition of the prepared material

3.4 FT-IR Analysis

The FT-IR spectrum of the synthesized CeO_2–TiO_2 nanocomposite displays characteristic vibrational bands that confirm the formation of the mixed-oxide structure and the presence of metal–oxygen linkages. The formation of metal–oxygen bonds was confirmed by FTIR analysis (Fig. 4).

A broad absorption band around 3430–3690 cm^{-1} corresponds to O–H stretching vibrations, which originates from physically adsorbed water molecules and surface hydroxyl functional groups. These hydroxyls are commonly present on the surface of metal oxides and play an important role in enhancing gas-sensing and photocatalytic responses by providing active adsorption sites. A weak band near 3100–3000 cm^{-1} may be associated with C–H stretching or residual organic traces from precursors or solvents used during synthesis.

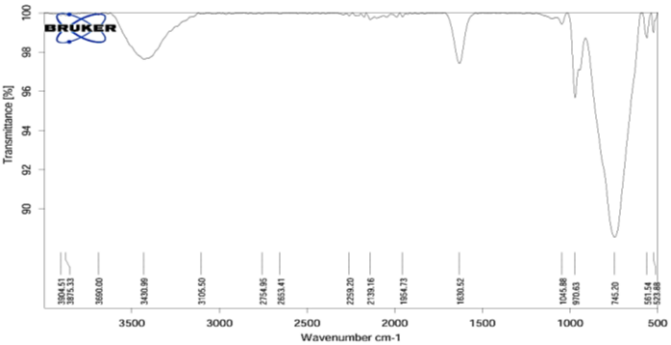

Fig. 4 FTIR spectrum of synthesized TiO_2–CeO_2 nanocomposite recorded in the range 4000–500 cm^{-1} showing characteristic metal–oxygen vibrational bands

The spectrum shows a minor but noticeable feature around 1630 cm^{-1}, which corresponds to H–O–H bending vibrations of molecular water bound to the nanoparticle surface. The small peaks at 2139 cm^{-1} and 1954 cm^{-1} may be attributed to atmospheric CO_2 absorption or weak overtones from surface species, commonly detected in metal-oxide FTIR spectra. No strong organic functional groups (such as C=O or C–N) are observed, indicating successful removal of organic residues during calcination.

The fingerprint region from ~400–800 cm^{-1} shows strong and broad transmittance dips, which are the most significant features of the spectrum. Peaks around 745 cm^{-1}, 970–1045 cm^{-1}, and the intense band at ~520–560 cm^{-1} correspond to combined Ti–O, Ti–O–Ti, and Ce–O stretching modes. The broad metal–oxygen absorption in this region is typical for nanosized CeO_2 and TiO_2, and the overlapping nature of these bands indicates the formation of an integrated CeO_2–TiO_2 nanocomposite. The slight shift in Ce–O and Ti–O bands relative to pure oxides suggests lattice distortion and strong interfacial interaction between Ce^{4+} and Ti^{4+} ionic sites, confirming composite formation at the nanoscale.

Overall, the FT-IR spectrum confirms the successful synthesis of the CeO_2–TiO_2 nanocomposite. The presence of strong metal–oxygen bands, surface hydroxyl groups, and the absence of undesired organic impurities affirm the purity of the sample and validate the structural integration of the two metal oxides. These structural features enhance surface reactivity, making the material suitable for applications in photocatalysis and gas sensing due to improved adsorption and charge–transfer capabilities.

3.5 XRD Analysis

The XRD pattern of the CeO_2–TiO_2 nanocomposite displays a prominent and sharp diffraction peak centered near $2\theta \approx 38°$, indicating the presence of a highly crystalline phase. The additional smaller peaks between 30°–35°, 55°–60°, and 65°–70° correspond to mixed phases of CeO_2 and TiO_2, suggesting successful incorporation of both metal oxides. The intense peak around 38° may correspond to the (111) plane of CeO_2 or the (004)/(112) reflections of TiO_2 depending on the exact structural ratio, indicating the dominance of one crystalline phase.

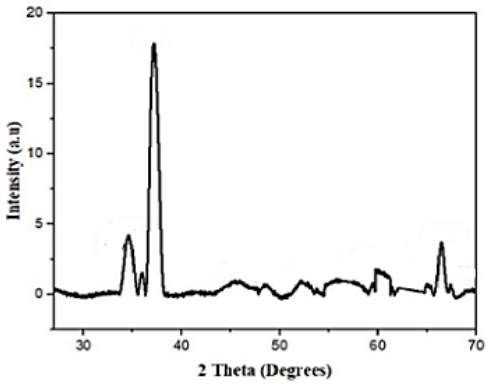

Fig. 5 X-ray diffraction (XRD) pattern of synthesized TiO_2–CeO_2 nanocomposite

The slight broadening of some peaks suggests nanocrystalline behaviour with small particle size, consistent with FE-SEM observations showing particle sizes around 20–33 nm. The crystalline structure was confirmed by XRD analysis (Fig. 5) The absence of impurity-related peaks confirms the high purity of the synthesized composite. The structural features, combined with peak broadening, imply lattice strain and strong CeO_2–TiO_2 interfacial interaction, which can significantly enhance photocatalytic and gas-sensing activity by facilitating charge separation and increasing defect density.

3.6 Gas Sensing Results

The CeO_2–TiO_2 nanocomposites exhibit excellent gas-sensing performance toward multiple gases, showing strong temperature-dependent sensitivity behavior. As the operating temperature increases from 40 °C to 200 °C, the overall sensitivity improves significantly. Among all tested gases, NO_2 shows the highest response, reaching more than 70% sensitivity at 200 °C, indicating strong oxidizing–reducing interactions between NO_2 molecules and the CeO_2–TiO_2 surface. H_2S also shows a notable response that gradually increases with temperature, achieving around 40% sensitivity at 200 °C. The temperature-dependent sensitivity is shown in Fig. 6a.

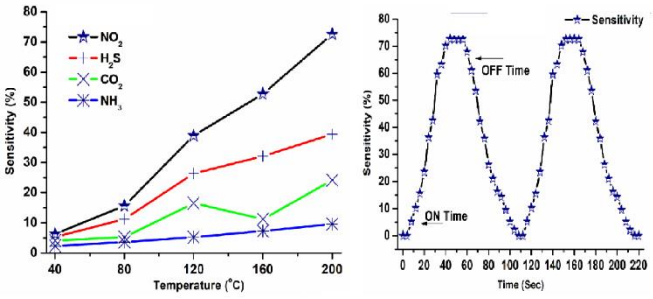

Fig. 6 a) Variation of gas sensitivity (%) of TiO_2–CeO_2 nanocomposite sensor toward NO_2, H_2S, CO_2, and NH_3 gases as a function of operating temperature (40–200 °C); and b) Dynamic response–recovery characteristics of the TiO_2–CeO_2 gas sensor showing sensitivity variation with time and indicating ON and OFF response cycles

https://doi.org/10.30799/jnst.S309.26110409

Cite this Article as: Hrutuja A. Patil, Gokul V. Suryawanshi, Tulshidas S. Savale, Synthesis and characterizations of CeO_2-TiO_2 nanocomposites for gas sensing applications, J. Nanosci. Tech. 11(4) (2026) 1153–1156.

CO_2 and NH_3 display moderate responses, with CO_2 showing a maximum near 120 °C followed by slight decline, while NH_3 shows a steadily increasing but comparatively lower sensitivity. This selective enhancement shows that the nanocomposite surface chemistry favours strong adsorption and reaction with NO_2 and H_2S gases.

Dynamic response curves further confirm the fast response and recovery behaviour of the CeO_2–TiO_2 sensor. During the ON cycle, sensitivity rapidly rises to its peak (~70%), demonstrating quick adsorption kinetics. In the OFF cycle, the signal smoothly returns to baseline, indicating efficient desorption and excellent reversibility. The dynamic sensing behaviour is illustrated in Fig. 6b. Repeated ON/OFF cycles maintain nearly identical peak heights, confirming high stability, reproducibility, and reliable long-term sensing performance. Overall, the CeO_2–TiO_2 nanocomposites show high sensitivity, fast response–recovery times, selective detection behaviour, and good cycling stability, making them promising candidates for practical gas-sensing applications, especially for NO_2 and H_2S detection.

4. Conclusion

Crystalline CeO_2/TiO_2 nanocomposites were synthesized via the sol–gel method and systematically characterized. XRD analysis confirmed well-defined crystalline phases with average crystallite sizes of 14–17 nm. At Ce/Ti ratios below 8/100, no distinct CeO_2 peaks were observed, indicating high cerium dispersion within the TiO_2 lattice, whereas higher Ce content (8/100–50/100) enhanced CeO_2 peak intensity and reduced anatase TiO_2 peak intensity. Lattice parameter variations confirmed structural modification due to Ceincorporation. XPS revealed Ti^{4+} as the dominant titanium species and mixed Ce^{3+}/Ce^{4+} states, promoting oxygen vacancies and improved charge transfer. UV–Vis spectra showed strong absorption at 350–380 nm, attributed to wide band-gap characteristics and defect states. FE-SEM analysis demonstrated porous nanosized grains (20–33 nm), while EDS and FT-IR confirmed chemical purity and successful composite formation. TheCeO_2/TiO_2 nanocomposites exhibited enhanced photocatalytic performance compared to pure TiO_2, particularly during the initial reaction stage, demonstrating their potential for photocatalytic and gas-sensing applications.

References

[1] M. Ijaz, M. Zafar, Titanium dioxide nanostructures as efficient photocatalyst: Progress, challenges and perspective, Int. J. Energy Res. 45 (2021) 3569-3589.

[2] D.R. Eddy, M.D. Permana, L.K. Sakti, G.A. Nur Sheha, Solihudin, Sahrul Hidayat, et al., Heterophase polymorph of TiO_2 (anatase, rutile, brookite, TiO_2(B)) for efficient photocatalyst: Fabrication and activity, Nanomaterials 13 (2023) 704.

[3] Gregor Žerjav, Krunoslav Žižek, Janez Zavašnik, Albin Pintar, Brookite vs. rutile vs. anatase: What's behind their various photocatalytic activities?, J. Environ. Chem. Eng. 10 (2022) 107722.

[4] Wei Zhang, Haili He, Haoze Li, Linlin Duan, Lianhai Zu, Yunpu Zhai, Wei Li, Lianzhou Wang, Honggang Fu, Dongyuan Zhao, Visible-light responsive TiO_2-based materials for efficient solar energy utilization, Adv. Energy Mater. 11 (2021) 2003303.

[5] Longbo Jiang, Shaoyu Zhou, Jinjuan Yang, Hou Wang, Hanbo Yu, et al., Near-infrared light responsive TiO_2 for efficient solar energy utilization, Adv. Funct. Mater. 32 (2022) 2108977.

[6] Khakemin Khan, Xiaoping Tao, Ming Shi, Bin Zeng, Zhaochi Feng, Can Li, Rengui Li, Visible-light-driven photocatalytic hydrogen production on $Cd_{0.5}Zn_{0.5}S$ nanorods with an apparent quantum efficiency exceeding 80%, Adv. Funct. Mater. 30 (2020) 2003731.

[7] X. Hu, G. Li, J.C. Yu, Design, fabrication, and modification of nanostructured semiconductor materials for environmental and energy applications, Langmuir 26 (2010) 3031-3039.

[8] Chaoqian Ai, Baoji Wang, Ke Duan, Jinyuan Jiang, Zeyu Jiang, et al., Enhanced photocatalytic activity by regulating charge transferring: Unveiling the decisive role of cerium oxide crystal-facet engineering over heterojunction, J. Colloid Interface Sci. 636 (2023) 341-350.

[9] S.G. Peera, S.W. Kim, Rare earth Ce/CeO_2 electrocatalysts: Role of high electronic spin state of Ce and Ce^{3+}/Ce^{4+} redox couple on oxygen reduction reaction, Nanomaterials 15 (2025) 600.

[10] Jian Tian, Yuanhua Sang, Zhenhuan Zhao, Weijia Zhou, Dongzhou Wang, et al., Enhanced photocatalytic performances of CeO_2/TiO_2 nanobelt heterostructures, Small 9 (2013) 3864-3872.

[11] Yuewu Huang, Zewu Xu, Changmiao Xie, Yanbin Yang, Xu Su, et al., Oxygen vacancy-engineered CeO_2/TiO_2 heterojunction for self-powered UV photodetection: Toward high-resolution imaging and reliable optical communication, J. Alloys Compd. (2025) 184320.

[12] Xiaoli Fan, Shiyao Wang, Yurong An, Woonming Lau, The enhancement of surface reactivity on CeO_2 (111) mediated by subsurface oxygen vacancies, J. Phys. Chem. C 120 (2016) 27917-27924.

[13] A.E. Danks, S.R. Hall, Z.J.M.H. Schnepp, The evolution of 'sol-gel' chemistry as a technique for materials synthesis, Mater. Horiz. 3 (2016) 91-112.

[14] Zhengjiang Liu, Dan Zhou, Huiyan Ma, Lei Xing, Qiancheng Zhang, Juming Liu, Sulfated CeO_2-TiO_2 as H_2 evolution photocatalyst: Synergic effects of heterojunction and sulfation on catalyst performance, J. Mol. Struct. 1314 (2024) 138732.

[15] Liping Wang, Yiyi Kang, Mingyuan Zhang, Yuxiao Liang, Jiali Liu, et al., Construction of a S-scheme oxygen-deficient CeO_2/TiO_2 heterojunction for efficient charge separation: Interfacial electronic behavior and mechanism insight, J. Alloys Compd. 1010 (2025) 177418.

[16] M. Humayun, C. Wang, W. Luo, Recent progress in the synthesis and applications of composite photocatalysts: A critical review, Small Methods 6 (2022) 2101395.

[17] Mingmei Li, Pengfei Wang, Zhezhe Ji, Zhiruo Zhou, Yuguo Xia, Yi Li, Sihui Zhan, Efficient photocatalytic oxygen activation by oxygen-vacancy-rich CeO_2-based heterojunctions: Synergistic effect of photoexcited electron transfer and oxygen chemisorption, Appl. Catal. B Environ. 289 (2021) 120020.

[18] Manoj Pudukudy, Qingming Jia, Jingyou Yuan, Sivagnanam Megala, Ramesh Rajendran, Shaoyun Shan, Influence of CeO_2 loading on the structural, textural, optical and photocatalytic properties of single-pot sol-gel derived ultrafine CeO_2/TiO_2 nanocomposites for efficient degradation of tetracycline under visible light irradiation, Mater. Sci. Semicond. Process. 108 (2020) 104891.

[19] D.P. Macwan, P.N. Dave, S. Chaturvedi, A review on nano-TiO_2 sol-gel type syntheses and its applications, J. Mater. Sci. 46 (2011) 3669-3686.

https://doi.org/10.30799/jnst.S309.26110409

Cite this Article as: Hrutuja A. Patil, Gokul V. Suryawanshi, Tulshidas S. Savale, Synthesis and characterizations of CeO_2-TiO_2 nanocomposites for gas sensing applications, J. Nanosci. Tech. 11(4) (2026) 1153–1156.